MSc in Photonics

PHOTONICS**BCN**

Universitat Politècnica de Catalunya (UPC)
Universitat Autònoma de Barcelona (UAB)
Universitat de Barcelona (UB)
Institut de Ciències Fotòniques (ICFO)

http://www.photonicsbcn.eu

Master in Photonics

MASTER THESIS WORK

Design and optimization of Photonic Systems for Microwave Applications

Daniel Nuño Gomez

Supervised by Dr. Santos Blanco, María Concepción, (UPC)

Presented on date 7th September 2017

Registered at

Escola Tècnica Superior d'Enginyeria de Telecomunicació de Barcelona

Design and Optimization of Photonic Systems for MicroWave applications

Daniel Nuño Gomez

I. Introduction

Extensively researched in the last years, the Microwave Photonics Technology field has a number of potential advantages including extremely wide bandwidth, very low frequency constant losses, light weight, immunity to EMI and high flexibility and tunability [1], being the telecommunications and the space industry one of the most benefited by these advantages [2]. This field has attracted both the interest of the scientific and commercial communities for almost 30 years, with remarkable success in the creation of new devices that can substitute the actual paradigm, mainly governed by electronics.

Despite the novelty of this technology, Microwave Photonic devices have already demonstrated astonishing features that outshine existing technology. Some of the most promising applications and advances in MWP are listed in [1]. MW Ultrawideband and arbitrary waveform generation at frequencies beyond 60GHz [3] with higher spectral purity than its electronic counterparts [4], THz-wave generation [5], beam forming for phased-arrayed antennas [6] [1] and MW signal filtering and processing are among the fields in which photonics has shown potential for overcoming the constraints of the actual technology. However, it also presents some serious challenges that must be overcome.

In this work, two representative examples of how photonics can be used to improve the performance of devices working at microwave frequencies are presented.

The first example is a Microwave Photonic Filter (MPF), a device used to filter RF signals while they are modulated in an optical carrier. MPFs have been proposed as an alternative to conventional microwave traditional filters based on cavities, transmission lines, etc, mainly because they hold promise for compact, lightweight devices with added performances such as wide tunability and high bandwidth [6].

As it will be shown, these type of MPFs can suffer from low stopband attenuation due to dispersion in the optical elements [7]. This main drawback is analyzed and modeled so the design can be optimized to lesen these disadvantages.

The MPF section is structured starting with a proposal provided by the literature [7]. Later, a new approach is proposed, which enhances the tuning capabilities and allows to minimize dispersion effects on the RF transfer function.

Also, a theoretical framework helpful in understanding the RF transfer functions obtained experimentally is provided and the phase characteristics of the optical filter are studied in order to limit the signal leakage of MPF in the stopband. The model has allowed to come up with an optimized filter design with improved characteristics. Both VPI Photonics and Matlab simulations and experimental results are shown to agree with the predictions provided.

The second example is a photonic correlator. Our proposal is specifically addressed for passive Interferometric Synthetic Aperture Radars (InSAR) imaging systems. Such systems employ large arrays of antennas to pick up natural thermal emission signals at microwave bands. Through time-correlation of each pair of signals and Fourier transformation, brightness temperature maps are obtained which provide information about the material properties of the objects in a scene. Practical applications usually require a large number of antennas which calls for imaginative solutions in order to reduce complexity and weight, specially for Earth observation applications. An example is the SMOS satellite, with a total of 72 receivers in a Y-shaped array working at 1.4 GHz [8]. A brief review of different proposals to exploit the properties of photonics in InSAR imaging systems is made, showing the main advantages and requirements of such setups.

In the proposed setup an optical signal is divided among all the receiver antennas in an array to be modulated with the microwaave signal received. Through photonic detection of each pair of signals a correlation signal at baseband is obtained so that after electronic fourier transformation the temperature map is retrieved. A main drawback of photonic approaches to passive imaging systems at microwave bands is that quickly varying random optical phase differences among optical signals coming from different receivers in the array must be compensated for. Even minimum thermal or mechanical perturbations can produce large phase changes due to optical path variation. Proposals based on feedback loops have a limited speed for error correction, requiring the feedback loop frequency to be at least 3 orders of magnitude higher than the error variation rate [9]. Other proposals require redundancy measurements in order to correct the phase error in real-time [10]. We present a technique for correcting the phase path differences in real-time without redundancy requirements.

Moreover, the proposed correlator is tested for the specific application of an Interferometric Synthetic Aperture Radar. Simulations done prove its correct operation as correlator, obtaining a stable signal output.

II. MPF State of the Art

From the many approaches explored so far, we may distinguish two broad categories, i. e. the incoherent and coherent kinds of MPF [11]. The former are based on incoherent sum of weighted delayed replicas of the signal, while the latter rely on modulation and optical filtering to smartly cancel some

of the optical signal sidebands in order to obtain the desired electrical transfer function. While incoherent approaches may provide full control over the RF transfer function characteristic via FIR arrangements, it is mostly at the expense of complex setups due to large number of taps required. Incoherent IIR approaches based on recirculating cavities provide an alternative to that, but in any case they require use of low-coherence sources such that the minimum delay time is longer than the coherence time and suffer from Phase-Induced Intensity Noise [11]. Because of this weighted sum operation, and the RF wave implicit periodicity, the RF transfer function obtained is frequency periodic, with minimum FSR given by the inverse of the taps delay times. Figure 1 shows the typical implementation of an incoherent FIR MPF with broadband source. Coherent approaches based on phase modulation and optical filtering on the other hand provide a single passband response, and very simple and compact setups, suited for integration. On the downside, their selectivity is usually lower and their constrains on dispersion of the optical setup are higher [12].

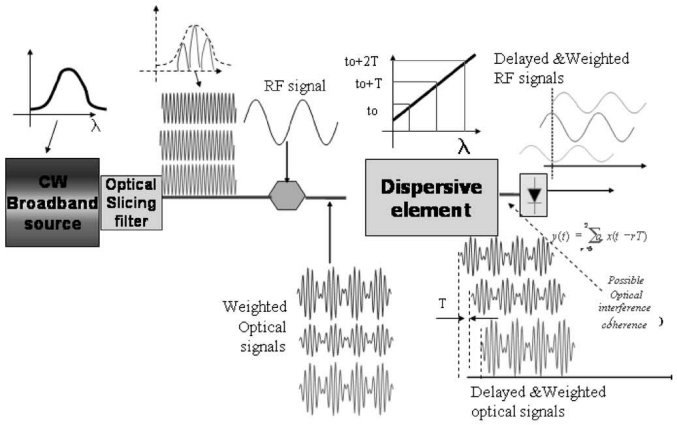

Fig. 1: Incoherent FIR MPF implementation. A broadband source is spectrally sliced, modulated and propagates through different delays.

A. MPF Principle of operation

The device is based on phase modulation of a laser beam with the microwave signal. Considering a small signal approximation ($m \ll 1$) for phase modulation, the optical electric field at the output of the modulator can be expressed as:

$$E_{mod}(t) = \sqrt{P_0}e^{j\omega_c t}\big(J_0(m) + J_1(m)e^{j\omega_m t} - J_1(m)e^{-j\omega_m t}\big) \tag{1}$$

Where P_0 stands for the optical power of light, ω_c the angular frequency of the optical carrier, ω_m the angular frequency of the modulation signal, $J_n(\alpha)$ the nth-order Bessel function of the first kind and m the phase modulation index.

The presented MPF depends on coherent interference of signals, and therefore the optical system transfer function, given by equation 2, has to be analyzed both in phase and amplitude.

$$\begin{aligned} H(\omega) &= A(\omega)\cdot e^{j\phi(\omega)} \\ E_F(\omega) &= E_{mod}(\omega)\cdot H(\omega) \end{aligned} \tag{2}$$

Where $A(\omega)$ is the attenuation of the filter and $\phi(\omega)$ is the systems phase response for any wavelength, then the signal after the optical filter is defined as $E_F(\omega)$. The optical phase of the system is defined with a Taylor expansion around the optical filter central frequency by equation 3.

$$\Phi(\omega) = \beta_1\omega + \frac{\beta_2}{2}\omega^2 + \frac{\beta_3}{6}\omega^3 \tag{3}$$

Where β_1 is equal to the time delay at ω_0, β_2 and β_3 are the second and third order Taylor coefficients and ω is the angular frequency difference with respect to the optical filter center.

The output current of a photodetector is proportional to the squared modulus of the optical electric field, given by equation 4.

$$I_d = |E_F|^2 \tag{4}$$

1) Single laser MPF: Figure 2 shows the optical setup and spectrum used for a single laser MPF. As can be seen in equation 1, the phase modulated signal has counter-phase modulated side-bands. The photodetected current can be obtained merging equations 1 and 4, obtaining two identical microwave signals in counter-phase as shown in equation 5. Therefore, photodetecting a signal without filtering will recover no microwave signal.

$$I_d = J_0J_1\big(2cos(\omega_{rf}t - \phi_0 + \phi_{0+}) - 2cos(\omega_{rf} + \phi_0 - \phi_{0-})\big) \tag{5}$$

Where the subindex $i = \{0,1\}$ refers to each one of the carriers, and $i_{\{+,-\}}$ is used to refer each one of the sidebands.

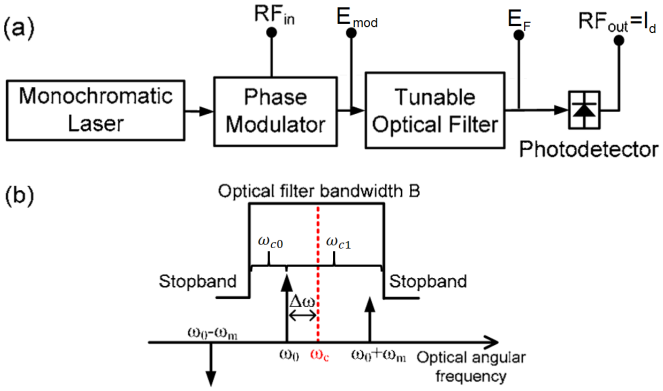

Fig. 2: Schematic and optical spectrum for a single laser MPF setup. ω_{ci} depict the RF cutoff angular frequencies delimiting the MPF passband.

Following the optical spectrum of figure 2 three different frequency regimes can be identified. Referred to the RF spectrum they can be labeled as lower stopband, passband, and upper stopband, which are related with the number of sidebands being attenuated by the optical filter. These regions are delimited by the cutoff frequencies, which can be expressed as $\omega_{c0} = \frac{BW_{opt}}{2} - \Delta\omega$ and $\omega_{c1} = \frac{BW_{opt}}{2} + \Delta\omega$, producing a

RF passband centered at $\frac{BW_{opt}}{2}$ with a RF bandwidth equal to $2\Delta\omega$.

The beating between each sideband and the carrier produces a sinusoidal wave, as shown in equation 5. If none sideband is attenuated, the signal detected is null as both cosines cancel each other.

However, as one of the sidebands is attenuated by the optical filter, the microwave signal can proportionally be recovered as its sideband counterpart is less destructively interfered, producing the passband of the MPF.

For frequencies above the bandpass, both sidebands are attenuated. The detected signal is therefore two counter-phased cosines which cancel each other, producing the upper stopband.

However, it can be seen in equation 5 that the signals produced by the sidebands have different phases. Therefore, dispersion in the optical setup produces this phase difference to slightly mismatch, reducing the attenuation of the MPF stopband. This is a main issue affecting these type of MPF as stopband attenuation might be highly reduced.

Dispersion might also affect the passband producing a ripple in the signal level due to the attenuated sideband interfering with the detected signal. As the interference is equally attenuated, the ripple produced is low, and its maximum value can be quantified by equation 6 .

$$Ripple_{II} = \sqrt{2P_0}Att \cdot J_0(m) \cdot J_1(m) \tag{6}$$

Where Att is the linear attenuation of the optical filter.

For frequencies above the bandpass, both sidebands are attenuated. As both sidebands have the same power level, this case is the same as for low frequencies. Therefore, even if dispersion is higher as sidebands are more frequency separated, its effects are attenuated and usually lower.

Figure 3 shows a simulation of the MPF transfer function, where the three regions can be identified. The blue line shows the signal detected if no optical filter is used, only due to dispersion, while the orange is the simulated transfer function. It can be seen that, for the lower stopband, the detected signal is equal to the signal detected without filtering, as the source of this signal is only dispersion. For the upper stopband, the source is the same but attenuated. Therefore, the transfer function in this region is attenuated by the same factor of the optical filter.

Now that its operation has been detailed, the detected photocurrent, defined in equation 5 is analyzed for each of the MPF bands. The different output signals can be summarized as in equations 7. The stopbands signal level is approximated taking only in account dispersion effects.

$$I_d = \begin{cases} \omega_{RF} < \omega_{c1} \rightarrow \sqrt{2P_0} \cdot J_0(m) \cdot J_1(m) \cdot \\ \qquad \cdot sin(\frac{\Phi_{0+}+\Phi_{0-}}{2} - \Phi_0) \\ \omega_{c1} < \omega_{RF} < \omega_{c2} \rightarrow \sqrt{2P_0} \cdot J_0(m) \cdot J_1(m) \\ \omega_{c2} < \omega_{RF} \rightarrow \sqrt{2P_0}Att \cdot J_0(m) \cdot J_1(m) \cdot \\ \qquad \cdot sin(\frac{\Phi_{0+}+\Phi_{0-}}{2} - \Phi_0) \end{cases} \tag{7}$$

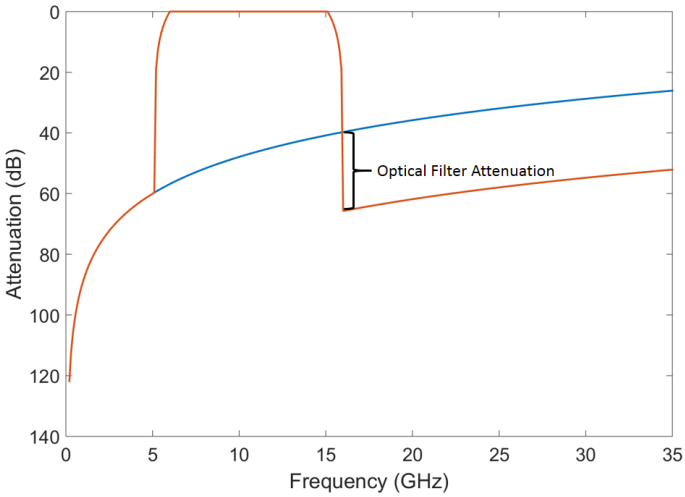

Fig. 3: Single laser MPF transfer function and non filtered signal leakage due dispersion.

This approach has been successfully developed in other MPF such as in [13] and [7]. Nevertheless, these systems require a tunable optical filter to acquire full tunability and also require the optical filter bandwidth to be the double of the MPF RF bandwidth. To comply this tunability constrain the setup uses thermally tuned Fiber Bragg Grattings. However, phase response of this optical filters become highly non linear near the bandpass limits. The higher the stopband attenuation and bandwidth [14] [15], the higher these no linearities are, which, as will be seen, dramatically affect the performance of the MPF.

2) Proposed MPF, double laser setup: Our approach reduces the requirements of the optical filter while keeping full tunability. Adding another laser source at the modulator input, other two pairs of counter-phase modulated sidebands appear in the optical spectrum. Figure 4 shows a diagram of the setup and the optical spectrum, where $\Delta\omega_i$ are the laser offsets with respect to the optical filter center and ω_{ci} are the cutoff RF angular frequencies delimiting the MPF passband. As there is no need of tuning the optical filter, Arrayed WaveGuide filters (AWG) can be used, which have a linear phase response inside the bandpass [15].

At low frequencies none sideband is attenuated. Each sideband produces a sinusoidal wave which is canceled with its counter-phased sideband wave, as shown in figure 5a. However, as in the single laser case, both groups of sidebands will dephase due to dispersion, producing part of the signal to be detected. Each pair of sidebands produces a different signal contribution, at the RF frequency and amplitude equal to the first case, detailed in equations 7. Nevertheless, both contributions have different phases, producing the resulting wave to have less amplitude. Treating each contribution as a phasor, the amplitude of the recovered signal is:

$$I_d(\omega_{RF} < \omega_{c0}) = \sqrt{2P_0} \cdot J_0(m) \cdot J_1(m) \cdot \left(\left|sin(\frac{\Phi_{0+}+\Phi_{0-}}{2} - \Phi_0) \cdot e^{j\frac{\phi_{0+}-\phi_{0-}}{2}} + sin(\frac{\Phi_{1+}+\Phi_{1-}}{2} - \Phi_1) \cdot e^{j\frac{\phi_{1+}-\phi_{1-}}{2}}\right|\right) \tag{8}$$

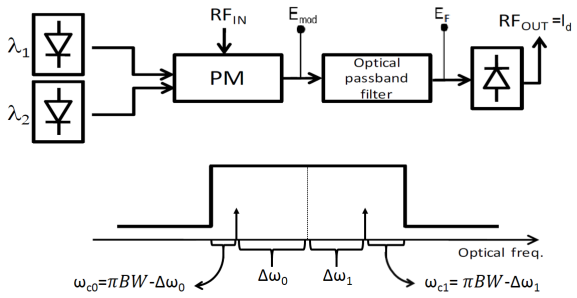

Fig. 4: MPF tunable filter setup proposal (top) and optical spectrum showing the laser emission inside the optical filter (bottom). $\Delta\omega_i$ are the laser offsets with respect to the optical filter center and f_{ci} are the cutoff RF frequencies delimiting the MPF passband.

It can be seen that if the phase difference between sidebands is smartly tuned, both contributions can counteract. This effect is analyzed in section II-C1 and can be used to optimize the MPF performance.

At RF frequencies between $\omega_{c0} < \omega_{RF} < \omega_{c1}$, the first sideband is attenuated and its partner sideband can be detected by the photodetector. This case is shown in figure 5b. One of the optical signals has one of its sidebands out of the filter passband, and is attenuated.

Therefore, photodetection produces a RF signal. The passband of the dual laser MPF is exactly equal to the single laser setup. Therefore, the passband signal level can be expressed as:

$$I_d(\omega_{c0} < \omega_{RF} < \omega_{c1}) = \sqrt{2P_0} \cdot J_0(m) \cdot J_1(m) \qquad (9)$$

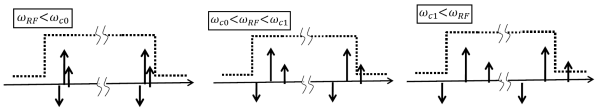

(a) Lower stopband. (b) Passband. (c) Upper stopband.

Fig. 5: Optical spectrum for the different frequency regimes of the RF filter.

As seen in figure 5c, for RF frequencies $\omega_{RF} > \omega_{c1}$ each carrier has an attenuated sideband. The resulting sidebands produce a RF signal upon photodetection, which destructively interfere. However, being each sideband from a different carrier, they are differently affected by dispersion. This counter-phased waver are more sensitive to the phase response of the optical filter, and takes in account not only the dephase between sidebands but also between carriers. Analyzing it, the signal power can be modeled as:

$$I_d(\omega_{c1} < \omega_{RF}) = \sqrt{2P_0} \cdot J_0(m) \cdot J_1(m) \cdot sin\left(\frac{\Phi_{0+} - \Phi_0 + \Phi_{1-} - \Phi_1}{2}\right) \qquad (10)$$

B. Experimental results

In order to prove the viability of the proposed MPF, the setup shown in figure 4 has been analyzed. The laser source used is a tunable NewFocus 6427C External Cavity Laser. Due to the lack of availability of two identical lasers, the response of the laser has been measured for different wavelengths and later combined with Matlab to obtain the final result. The Phase Modulator is an electro-optical Lithium Niobate modulator with 35 GHz bandwidth and V_π=5.5V. An Agilent 8510D Vector Network Analyzer with 42 GHz bandwidth is used as RF input and output to characterize the capabilities of the system. A Finsar 1000s WaveShaper is used to perform any desired type of optical filter, which has a resolution of 10 GHz. It is programmed to act as a 200 GHz rectangular filter. The limited frequency resolution of the WaveShaper will limit the steepness of the resulting transfer function.

1) Optical Filter: Figure 6 shows the transfer function and the group velocity dispersion of the used optical filter. To measure the dispersion of the filter, the MPSM method has been used [16]. A near flat group delay is appreciated, except for the edges of the stopband. However, the phase response in this region can be neglected as signals here are attenuated and do not need to keep its phase to cancel.

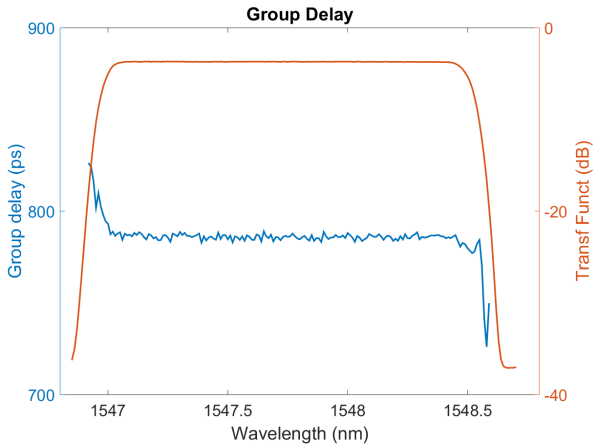

Fig. 6: Optical filter transfer function

Different optical filter approaches have been tested with almost identical results. An rectangular 180°phase shift filter has the ability to take advantage of the power of both sidebands, coherently adding both contributions instead of rejecting one of them. However, the phase change, equivalent to the stopband edge, are less prominent and the steepness of the MPF is worst.

2) RF Filter: This section shows the measured transfer functions of the MPF implemented. Figures 7a and 7b show different MPF realizations, demonstrating the tunability of the filter. Figure 7a shows different high pass filters by tunning the first cutoff frequency, while 7b shows tunning of the second cutoff frequency.

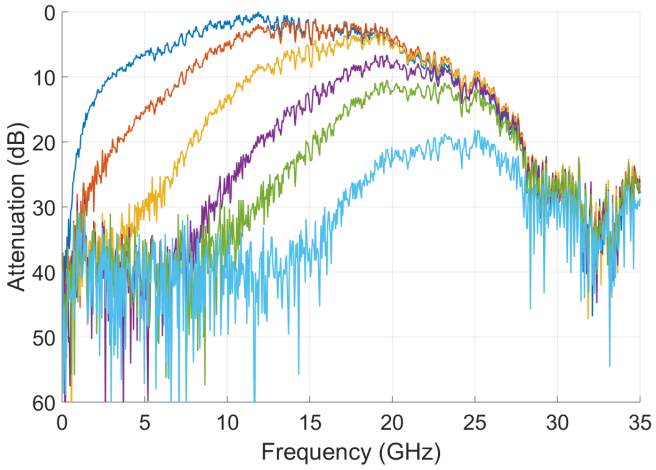

(a) The laser nearest the optical filter transition band is wavelength tuned in order to change the lower MPF cutoff frequency

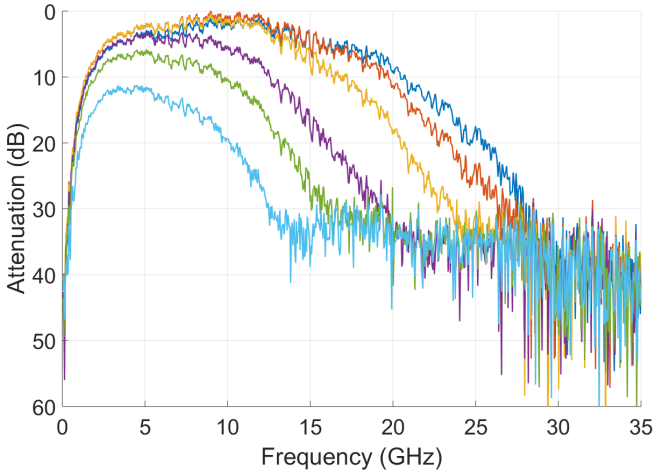

(b) The laser farthest to the optical filter transition band is tuned in order to change to higher cutoff frequency

Fig. 7: RF measured filter transfer functions for different laser detunings.

Any combination of first cutoff frequency with other second cutoff frequency is also achievable, performing bandpass filters centered at any desired frequency.

The linearity of the filter has been analyzed. Input powers up to 20 dBm proving to perform linearly for all input powers available.

C. MPF model analysis

Simulations done in VPI Photonics and Matlab show that our model is able to predict the resulting RF transfer function accurately, taking equations 7, 8, 9 and 10 as base.

The most relevant features can be summarized in function of its sources, which are also delimited to the MPF bands (low frequency stopband, passband, and high frequency stopband).

For a *single laser setup*, the signal leakage is produced by a single pair of sidebands. Therefore, the signal level in the lower stopband is equal to the detected level without filtering. As shown in figure 3, the upper sideband is equal to the signal without filtering but attenuated. The RF passband, which amplitude can be approximated by equation 7, is an scaled replica of the optical filter passband.

In the *dual laser setup* the passband remains as an scaled replica of the optical filter transfer function with same amplitude, also defined by 7. Nevertheless, dispersion effects are more complex. As shown in equations 8 and 10, each modulated carrier has its own contribution. Although this can produce a higher signal leakage, it can be used in order to reduce it if this contributions are not in phase, largely increasing the MPF performance if correctly tuned. Therefore, the analysis of the optical system phase response allows us to tailor the dispersion effects by changing it, using different filters or adding dispersive elements to the setup.

In both implementations a secondary passband, with half the bandwidth and half the center frequency of the main passband, is produced by beatings between higher order sidebands, which have amplitudes equal to $J_2(m)$. The secondary passband is typically under the noise level and therefore can be neglected. The relation between passband levels can be expressed as $\frac{J_0(m)}{J_2(m)}$, which for typical values used in our simulations produce secundary passbands 80 dB under the main passband level. However, if an optical system with very low dispersion, dispersion compensation techniques are used or a very high modulation index (m) is used, it might be detectable. Therefore, there is a trade off between the attainable attenuation and the dynamic range of the filter.

1) Intrinsic dispersion compensation in dual laser setup: Signal leaking in the low frequency stopband of the dual laser setup come from different contributions. It can be shown that exists a relation between the optical phase Taylor terms and the laser detunings which ensures both signals cancel each other.

The optical phase constrains to ensure both phases are counter-phased are quite complex. However, it is possible to ensure that both amplitudes are equal but with opposite sign and the phases are equal. Developing the realation $sin(\frac{\Phi_{0+}-\Phi_{0-}}{2}) = -sin(\frac{\Phi_{1+}-\Phi_{1-}}{2})$, which can be expressed by $\Phi_{0+} - \Phi_{0-} = -(\Phi_{1+} - \Phi_{1-})$ and taking advantage of equation 3 the relation for the phase of the signals can be obtained.

Furthermore, if the amplitude of both contributions is analyzed, the expression that ensures that both amplitudes are equal and with opposite sign obtained is exactly the same, and is defined by equation 11.

$$BW_{RF} \cdot \pi = \frac{\Delta\omega_0 - \Delta\omega_1}{2} = \frac{\beta_2}{\beta_3} \tag{11}$$

Being $\Delta\omega_i$ the detuning offsets of each laser with respect to the center of the optical filter.

Considering the second stopband, now the expression to minimize in order to ensure the signal power in the stopband is minimum is $sin\left(\frac{\Phi_{0+}-\Phi_0+\Phi_{1-}-\Phi_1}{2}\right)$. Using equation 3 and 10, the phase response requirements can be expressed as in equation 12.

$$BW_{RF} \cdot \pi = \frac{\Delta\omega_0 - \Delta\omega_1}{2} = \frac{\beta_2}{\beta_3} \tag{12}$$

Which is exactly the same expression as for minimizing the dispersion effects on the low frequency stopband, allowing for simultaneous cancellation of dispersion signal leakage in both stopbands.

Therefore it is possible to add dispersive elements to the optical system in order to improve the MPF attenuation at the stopbands. Simulations in both Matlab and VPI Photonics agree with this prediction, demonstrating dispersion immunity is acquirable if the requirements are well met.

Figure 8 shows the simulation results for four different optical phases, where the yellow line depicts the result for an optimized dispersion, while the other optical filters have lower dispersion values (blue and orange lines have 100 and 10 times lower β_3 respectively, and the violet line shows a system with $\beta_3 = 0$ and β_2 10 times lower). As can be seen, the optimized optical phase system shows a highly improved stopband attenuation compared with the other implementations. The secondary passband, produced by beatings with higher order sidebands is easily detected in the optimized implementation. Figure 9 shows the optical phase of each of the implementations.

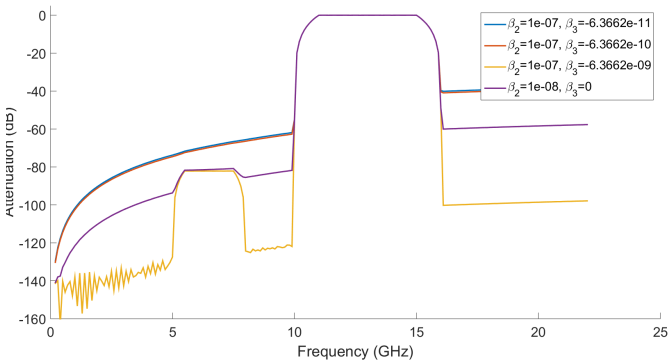

Fig. 8: MPF RF Transfer Functions for different optical filter phases. Yellow line is the result of an optimized optical phase.

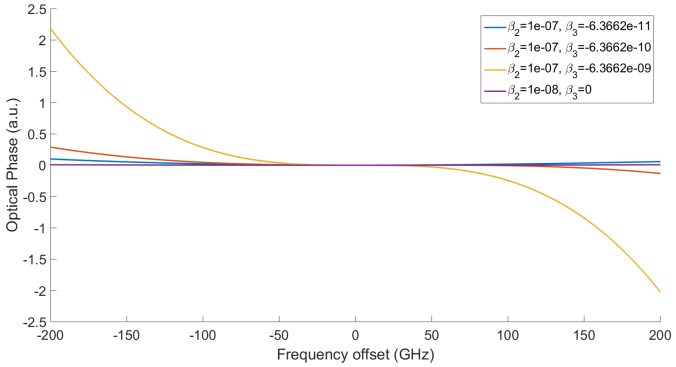

Fig. 9: Optical filter phases used to obtain the results shown in figure 9.

III. Optical Correlator for inSAR imaging applications and Phase Correction Methods

Correlators are devices which compute the cross-correlation between two signals (defined by equation 13). They are useful to detect the similarity of the received signal with the different expected pulses in any telecommunications system, but can also be used for a wide number of applications. One of them is Interferometric Synthetic Aperture Radars. These devices are formed by an array of antennas, for which the correlation between each antenna is computed and used to obtain the scene image. With this procedure, the resolution of the array is equivalent to which an antenna the size of the maximum separation between antennas in the array would have. Furthermore, the reconstructed image has spatial resolution, in comparison with an equivalent bigger antenna which would only provide the total radiation power detected. Figure 10 depicts how an inSAR is capable of obtaining spatial resolution from the phase difference of the received signals.

$$f(t) * g(t)(\tau) = \int_{-\infty}^{\infty} f^*(t)g(t+\tau)dt \tag{13}$$

The correlation of each pair of antennas is related with the spatial frequency equal to its separation. Therefore, if all pairs of correlations are related to its spatial frequencies, the Fourier Transform of the scene image is obtained (which is known as the visibility function) [17]. It can be seen as if each pair of antennas perform a sampling of their related spatial frequency, and the image is then reconstructed from it.

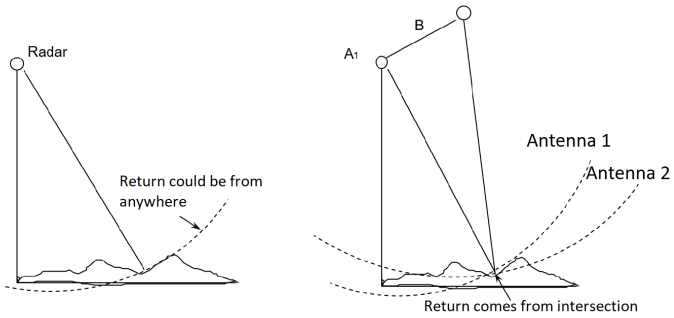

Fig. 10: Comparison between Total Power Radiometer and inSAR implementation.

Being for InSAR or for any other application, if a conventional electronic approach is used, the sampling rate needed to accomplish the Nyquist theorem might be so high that commercial devices could not be available, while Ultra-high bandwidth electro-optical modulators of up to 300 GHz [18] have been demonstrated. Furthermore, electric signal distribution above 67 GHz approximately require the use of metallic waveguides [19]. This implies a huge increase in the bandwidth capabilities of any optical implementation.

Therefore, in an InSAR system, three steps can be distinguished: Signal acquisition and distribution, pair correlation and Fourier Transform. There are different approaches to photonic imaging systems depending on the level of photonic implementation for these steps. Photonics can provide a number of advantages for these devices, but may also imply

hard requirements. One common requirement for devices using photonic technologies for anything more than signal distribution is the phase difference between antenna signals. In order to obtain the correlation of each pair of signals, they must be mutually coherent. At optical wavelengths, however, random phase changes can be added from many different sources. Thermal changes and vibrations specially affect, changing the effective optical path of the signal. In order to compensate this, different proposals have been done that can recover the optical phase information needed.

Figure 11 shows the setup proposed in [20], a whole photonic setup is used. Each antenna signal is phase-modulated and coupled to a fiber. The fiber array has to be exactly positioned as a scale model of the antenna array, and a lens is used to obtain the Fourier Transform of all the signals at its focal point, where a CCD camera is used to recover the image. Figure 11 shows the setup proposed in [20]. This procedure takes advantages of all the photonic benefits, as extremely high bandwidth and low losses and weight. However, this implementation has three requirements. First, a phase compensation method to overcome random fluctuations in the relative optical phases. Second, the fibers must be perfectly arranged to form a scaled version of the antenna array. And third, a single sideband modulation has to be done in order to obtain the image with unambiguity, which increases the system complexity.

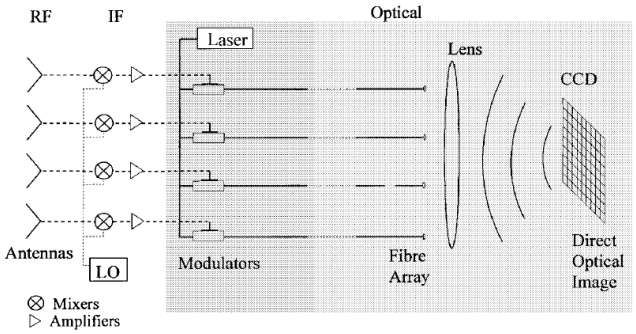

Fig. 11: All optical InSAR setup.

In this proposal, Blanchard uses a method to compensate the phase fluctuations called Redundant Spacing Calibration [10]. It takes advantage that pairs of antennas that have the same spatial separation are measuring the same spatial frequency, thus reducing the number of unknowns to solve the relative phase errors.

Stochastic Parallel Gradient Descent (SPGD) is technique for optical phase correction. It was first proposed in [21], and has been widely used since then, as in [22] and [9]. This procedure uses a feedback-loop to detect the phase difference between both signals. Then, a DC voltage proportional to the phase error is injected in one of the phase-modulators, so the phase difference is compensated. However, the faster the phase can vary, the faster the feedback-loop must go to compensate it correctly. It is shown in [9], that the feedback frequency needed scales proportionally to the bandwidth of the phase error, requiring 1 KHz of feedback frequency for each 1 Hz of phase error bandwidth.

Another important proposal is the ESA satellite SMOS, carrying the MIRAS payload which is a MicroWave Interferometer Radar with Synthetic Aperture. Space technologies must pass high reliability tests and use well known technologies, so this SAR uses only photonics to distribute the MW signal while both correlation and Fourier Transformation are carried out electronically [8].

E. Nova develops a photonic correlator for SAR imaging devices with an implementation similar to this work [25]. It takes advantage of optical signal distribution and interference between optical signals in order to obtain a RF signal whose power is proportional to their complex correlation. Therefore, the correlation is done in the MW domain but reducing the requirements for the electrical signal processing.

	Signal Distrib	Optical interference	Correlation	FT	Image retrieval
SMOS	✓	✗	✗	✗	✗
E. Nova	✓	✓	✗	✗	✗
This work	✓	✓	✓	✗	✗
Blanchard	✓	✓	✓	✓	✓

TABLE I: Depth of photonic implementation in different proposed SAR imaging systems.

Table I shows how the detailed systems take advantage of photonics for signal processing. In our proposal, photonics is exploited up to the correlation measurement. After that, the signals are treated electronically, and specifically the Fourier transformation is carried out in the electronic domain, as in traditional approaches. This has the added advantage of allowing estimation of the phase path differences that the signals coming from each antenna acquire while they travel independently from each antenna, using all the information contained into the optical signal, such as the different spectral components and different polarizations.

A. Optical Correlator proposal and path difference compensation technique

The proposal of this work implements optical signal distribution and optical correlation, while leaving the Fourier Transform and image reconstruction to the electronic domain. This way the severe alignment requirements for the optical Fourier Transform are eliminated, which also provides a more robust setup against vibrations and simplifies the setup avoiding the use of lenses. Also, by computing the correlations in the optical domain this setup avoids many heavy electrical components, thus reducing the weight and keeping high bandwidth capabilities. The most acute drawback is the need to keep the phase coherence between the optical signals coming from antennas that need to be physically apart from each other. Figure 12 shows the setup for our proposal in the VPI Photonics simulator software. In a practical implementation,

The signal from one laser is divided and sent towards each antenna in the array to be modulated with the corresponding RF signal. Once the modulated signals are coupled the random differences between the optical path lengths traveled from each antenna must be compensated. Each antenna is simulated by a

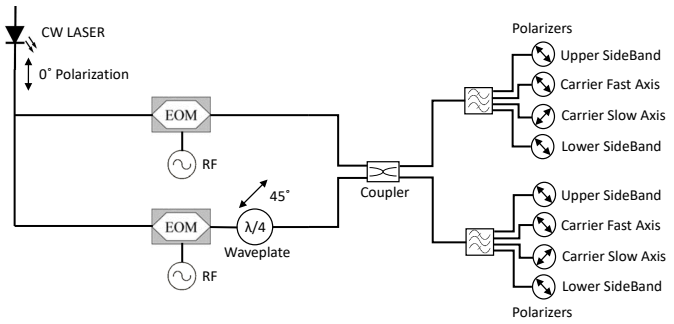

Fig. 12: Proposed setup for optical correlator with Fourier Transform in the electrical domain. Optical phase difference information can be obtained by analysis of the different bands power.

sinusoidal wave, which can have different phases to simulate a moving source. Hence, the modulating signal can be expressed as $V_R = V_i cos(\omega_r t + \theta_1)$, which after being up-converted to the optical domain yields two modulated electric fields described by equations 14.

$$\begin{aligned} E_1(t) &= E_0 e^{j\phi_1}(1 + j\beta_1 e^{j(\omega_r t+\theta_1)} - j\beta_1 e^{-j(\omega_r t+\theta_1)}) \\ E_2(t) &= E_0 e^{j\phi_2}(1 + j\beta_2 e^{j(\omega_r t+\theta_2)} - j\beta_2 e^{-j(\omega_r t+\theta_2)}) \end{aligned} \tag{14}$$

Where $\beta_i \approx \frac{m}{2} = \frac{\pi V_R}{2V_\pi}$ (being m the modulation index V_R the RF amplitude and V_π the voltage required by the modulator for a π phase change), ω_r the angular frequency of the modulating signal and ϕ_i the optical phase change due to propagation. One of the optical signals of the pair goes through a quarter-wave plate oriented at 45 °with respect to the laser polarization. Therefore, from now on two polarizations will be considered separately, the one in the direction of the quarter-wave plate fast axis and in the direction of the slow axis. Therefore, two sets of coupled signals are available at different polarizations, one of which has been delayed $\pi/2$. This is necessary to obtain the relative phase difference with unambiguity as it will be seen.

A coupler is used to join both signals, and a narrow-band Arrayed Wave Guide filter is used to isolate each sideband and carrier. Linear polarizers are used to filter the polarization which went through the fast axis on the quarter-wave plate and the one which went through the slow axis, and the power of each branch is measured.

Being the transmission matrix of a coupler $M = \frac{1}{\sqrt{2}}\begin{pmatrix} 1 & j \\ j & 1 \end{pmatrix}$, then the complex amplitudes of each filtered branch are defined by equations 15. For simplicity, only the fast axis polarization is analyzed now.

$$\begin{aligned} E_{C1} &= e^{j\phi_0} + je^{j\phi_1} \\ E_{USB1} &= j\beta_1 e^{j\phi_0} e^{j(\omega_r t+\theta_1)} - \beta_2 e^{j\phi_1} e^{j(\omega_r t+\theta_2)} \\ E_{LSB1} &= j\beta_1 e^{j\phi_0} e^{-j(\omega_r t+\theta_1)} - \beta_2 e^{j\phi_1} e^{-j(\omega_r t+\theta_2)} \\ E_{C2} &= je^{j\phi_0} + e^{j\phi_1} \\ E_{USB2} &= -\beta_1 e^{j\phi_0} e^{j(\omega_r t+\theta_1)} + j\beta_2 e^{j\phi_1} e^{j(\omega_r t+\theta_2)} \\ E_{LSB2} &= -\beta_1 e^{j\phi_0} e^{-j(\omega_r t+\theta_1)} + j\beta_2 e^{j\phi_1} e^{-j(\omega_r t+\theta_2)} \end{aligned} \tag{15}$$

Where Ci refers to the carrier amplitude, $USBi$ for the Upper SideBand amplitude and $LSBi$ for the Lower Sideband Amplitude. Therefore, measuring the power of each branch yields the values expressed in equations 16.

$$\begin{aligned} P_{C1} &= I_0(2 + 2sin(\Delta\phi)) \\ P_{USB1} &= I_0(\beta_1^2 + \beta_2^2 + 2\beta_1\beta_2 sin(\Delta\phi + \Delta\theta)) \\ P_{LSB1} &= I_0(\beta_1^2 + \beta_2^2 - 2\beta_1\beta_2 sin(-\Delta\phi + \Delta\theta)) \\ P_{C2} &= I_0(2 - 2sin(\Delta\Phi)) \\ P_{USB2} &= I_0(\beta_1^2 + \beta_2^2 - 2\beta_1\beta_2 sin(\Delta\phi + \Delta\theta)) \\ P_{LSB2} &= I_0(\beta_1^2 + \beta_2^2 + 2\beta_1\beta_2 sin(-\Delta\phi + \Delta\theta)) \end{aligned} \tag{16}$$

From these band powers the variables I_0 and $sin(\Delta\phi)$ are easily obtained as:

$$\begin{aligned} I_0 &= \frac{P_{C1} + P_{C2}}{4} \\ sin(\Delta\phi) &= \frac{P_{C1} - P_{C2}}{4} \end{aligned} \tag{17}$$

However, there are two issues with this approach. As only the value of $sin(\Delta\phi)$ is obtained, there is an ambiguity of $\pm\pi$ in the measure of $\Delta\phi$ which translates in a sign ambiguity in the value of $cos(\Delta\phi)$, preventing to obtain the imaginary part of the complex correlation. A second issue is that, for values of $sin(\Delta\phi) \approx 0$ a small error in the measure produces a high error in the $\Delta\phi$ measure, corrupting the correlation result.

Analyzing the slow axis polarization, it can be seen that with respect to the fast axis polarization, the carriers have an extra $\pi/2$ dephase. Hence, the new optical phase difference is $\Delta\phi' = \Delta\phi - \pi/2$ and $sin(\Delta\phi') = -sin(\pi/2 - \Delta\phi) = -cos(\Delta\phi)$. Consequently, the value of $cos(\Delta\phi)$ can be obtained with unambiguity applying equation 18.

$$cos(\Delta\phi) = \frac{P_{C2B} - P_{C1B}}{4} \tag{18}$$

Where P_{CiB} are the detected power for each carrier in the slow axis polarization. Hence, the complex correlation can be computed with equations 19.

$$\begin{aligned} \Re\{Correlation\} &= \beta_1\beta_2 cos(\Delta\theta) = \frac{P_{USB2} - P_{LSB1}}{4I_0 sin(\Delta\phi)} \\ \Im\{Correlation\} &= \beta_1\beta_2 sin(\Delta\theta) = \frac{P_{USB1} - P_{LSB1}}{4I_0 cos(\Delta\phi)} \end{aligned} \tag{19}$$

For antenna pairs which both have or both lack the quarter-wave plate, the phase difference can not be directly measured. However, it is possible to obtain it by relating their phase difference to other two pairs which phase difference is known.

1) Phase correction algorithm: Even knowing simultaneously $cos(\Delta\phi)$ and $sin(\Delta\phi)$ whenever values of either $cos(\Delta\phi)$ or $sin(\Delta\phi)$ are near 0, substantial errors and sign changes can appear.

To avoid this issues, an algorithm reconstructs the correlation result after detection. For each data value with $cos(\Delta\phi)$ or $sin(\Delta\phi)$ near 0, the relation $sin^2(\phi) + cos^2(\phi) = 1$ is applied to correct the possible error.

A second part of the algorithm checks for errors in the sign. Whenever the values of $sin(\Delta\phi)$ or $cos(\Delta\phi)$ are near 0, the

complex correlation will be far from 0. Therefore, if a sample of the complex correlation has different sign that one of its neighbor samples, the sign is changed.

Figure 13 shows the evolution of the phase difference between optical signals in a simulation on VPI over 64 nanoseconds.

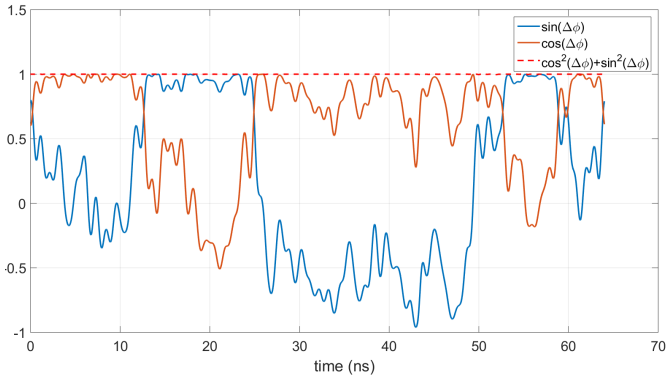

Fig. 13: Evolution of the phase difference between optical signals. The function $sin^2(\phi) + cos^2(\phi)$ is plotted to validate the data.

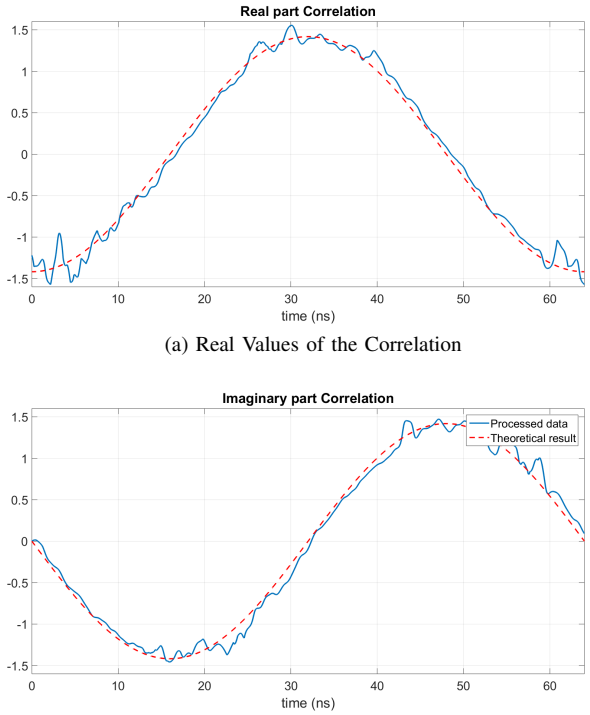

(a) Real Values of the Correlation

(b) Imaginary values of the Correlation

Fig. 14: Correlation results for a MW source in movement. The phase between each antenna signal changes from 0 to 2π radians.

B. Results

To prove the operation of the optical correlator device, the setup shown in figure 12 has been modified so one of the microwave generators has a progressive phase difference starting at 0 radians up to 2π radians. This simulates an inSAR system with two antennas focusing a point source in movement. The results are shown in figure 14. The blue line depicts the results obtained, while the red dashed line is the theoretical curve. The results match the expected outcome with minimum deviations, validating both the correlator setup and the error correction algorithm.

The correlator has been also tested as a part of a 2, 4 and 8 antenna array with InSAR implementation. Different microwave generators with variable phase shift simulate a source in motion. The correlations performed have been used to reconstruct the visibility function of the scene, which has been Fourier anti-Transformed in order to obtain the brightness temperature image of the scene. The produced image agrees with a point source in constant movement. However, some variations in the movement rate and the brightness of the source can be seen.

The Point Spread Function (PSF) of the 4 and 8 antenna arrays has been studied. Figure 15 show the simulated PSF for arrays of 4 and 8 antennas.

The operation of the inSAR algorithm obtains an image of the scene with angular resolution, as shown in figure 15. The angular resolution given by an inSAR array is proportional to the wavelength and maximum separation between antennas (A), and therefore the horizontal axis is shown to be $cos(A/\lambda)$.

IV. Conclusions

A new Microwave Photonic Filter structure with full tunability and single passband has been demonstrated. While needing two laser sources, it keeps a low system complexity and high versatility as tunability is achieved by the laser emission wavelength with a fixed optical filter. Thus allowing to focus on designing the optical filter with optimum characteristics.Furthermore, the MPF is capable of dispersion effects compensation, producing outstanding attenuations in the stopband. In comparison with the single laser setup, our proposal can take advantage of the optical phase response of the system in order to minimize dispersion effects that reduce the stopband attenuation. Simulations have been done that prove that with an adequate optical filter very high selectivity and tunability can be achieved. Also, the simulation model developed can reproduce the resulting RF transfer function and provides a useful tool for optimization of the filter design.

In the other hand, the optical correlator developed takes advantage of most of the benefits of photonics without the main drawbacks that some implementations require, as exactly positioning of the fiber array. The main drawback is the random phase fluctuations, for which different techniques have been developed. This techniques usually depend in a feedback loop or in elements redundancy. Our proposal for the phase control is able to compensate fluctuations in the phase difference in real time without redundancy, nor feedback loops, which require a minimum speed in order to compensate fast fluctuations. The device is proven to operate as expected, with simulations agreeing with the theory. An specific application for the correlator has been tested with good results, and the implemented phase control can be used for other photonic applications.

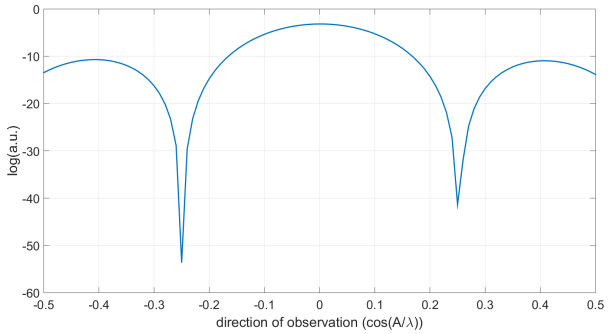

(a) Point Spread Function for an array of 4 antennas

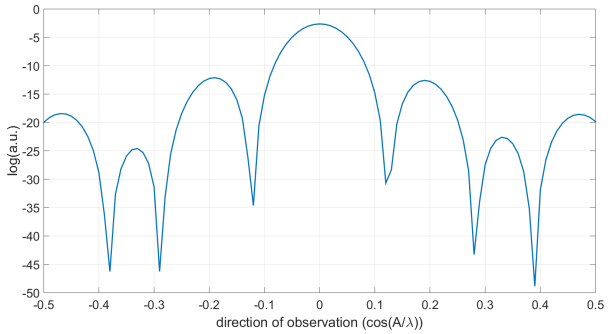

(b) Point Spread Function for an array of 8 antennas

Fig. 15: Simulated PSFs for different arrays of antennas, where A is the maximum separation between antennas.

REFERENCES

[1] J. Capmany and D. Novak, Microwave photonics combines two worlds, Nature Photon., vol. 1, pp. 319330, 2007.

[2] Vono, S., et al. "Towards telecommunication payloads with photonic technologies." International Conference on Space Optics. Vol. 7. 2014.

[3] M. Kahn, H. Shen, Y. Xuan, L. Zhao, S. Xiao, D. Leaird, A. Weiner, andM. Qi, Ultrabroad-bandwidth arbitrary radiofrequency waveform generation with a silicon photonic chip-based spectral shaper, Nature Photon., vol. 4, pp. 117122, 2009.

[4] Clark, Thomas R., and Rodney Waterhouse. "Photonics for RF front ends." IEEE microwave magazine 12.3 (2011): 87-95.

[5] J.-M. Wun et al., Photonic high-power continuous wave THz-wave generation by using flip-chip packaged uni-traveling carrier photodiodes and a femtosecond optical pulse generator, J. Lightw. Technol., vol. 34, no. 4, pp. 13871397, Feb. 15, 2016

[6] J. Capmany, J. Mora, I. Gasulla, J. Sancho, J. Lloret, and S. Sales, "Microwave Photonic Signal Processing," J. Lightwave Technol. 31, 571-586 (2013)

[7] T. Chen, X. Yi, L. Li, and R. A. Minasian, Single passband microwave photonic filter with wideband tunability and adjustable bandwidth, Opt. Lett. 37(22), 46994701 (2012)

[8] Palacio, Rafael, Franois Deborgies, and Petri Piironen. "Optical distribution of microwave signals for Earth observation satellites." Microwave Photonics (MWP), 2010 IEEE Topical Meeting on. IEEE, 2010.

[9] He, Yuntao, et al. "Optical phase control for MMW sparse aperture upconversion imaging." Chinese Optics Letters 12.5 (2014): 051101.

[10] Blanchard, Paul M., et al. "Phase calibration of arrays at optical and millimeter wavelengths." JOSA A 13.7 (1996): 1593-1600.

[11] Capmany, J., Ortega, B., and Pastor, D. (2006). A tutorial on microwave photonic filters. Journal of Lightwave Technology, 24(1), 201-229.

[12] Yao, J. (2009). Microwave photonics. Journal of Lightwave Technology, 27(3), 314-335.

[13] Yi, X., and R. A. Minasian. "Microwave photonic filter with single bandpass response." Electronics letters 45.7 (2009): 362-363.

[14] Kashyap, Raman. Fiber Bragg gratings. Academic press, 2009.

[15] Lenz, G., et al. "Dispersive properties of optical filters for WDM systems." IEEE journal of quantum electronics 34.8 (1998): 1390-1402.

[16] Moral Cerezo, F., Ferrer Picon, X. "Diseo y puesta en marcha de un banco de medidas de dispersin a frecuencias pticas" (2009)

[17] Corbella, I., Duffo, N., Vall-Llossera, M., Camps, A., and Torres, F. (2004). The visibility function in interferometric aperture synthesis radiometry. IEEE Transactions on Geoscience and Remote Sensing, 42(8), 1677-1682.

[18] Shi, Shouyuan, et al. "System modeling of passive millimeter wave imager based on optical up-conversion." SPIE OPTO. International Society for Optics and Photonics, 2012.

[19] Dennis W. Prather, "Photonic Materials and Devices for RF (mmW) Sensing and Imaging", University of Delaware (2012)

[20] Blanchard, P. M., et al. "Coherent optical beam forming with passive millimeter-wave arrays." Journal of Lightwave Technology 17.3 (1999): 418.

[21] M. A. Vorontsov and V. P. Sivokon, "Stochastic parallel-gradient-descent technique for high-resolution wave-front phase-distortion correction," J. Opt. Soc. Am. A 15, 2745-2758 (1998)

[22] K. Underwood, A. Jones, and J. Gopinath, "FPGA-based phase control of acousto-optic modulator Fourier synthesis system through gradient descent phase-locking algorithm," Appl. Opt. 54, 5624-5628 (2015).

[23] R. A. Minasian, E. H. W. Chan, and X. Yi, "Microwave photonic signal processing," Opt. Express 21, 22918-22936 (2013)

[24] Minasian, R. A. "Ultra-wideband and adaptive microwave photonic signal processing." Transparent Optical Networks (ICTON), 2015 17th International Conference on. IEEE, 2015.

[25] Nova Lavado, Enrique. "Millimeter-wave and terahertz imaging techniques." (2013).